Differential expression of acidic proteins with progression in the MCF10 model of human breast disease

NATHAN S. BUCHANAN[1], JIA ZHAO[1], KAN ZHU[3], TASNEEM H. PATWA[1],
FRED R. MILLER[4] and DAVID M. LUBMAN[2]

Departments of [1]Chemistry, [2]Surgery, The University of Michigan, Ann Arbor, MI; [3]Novartis Institute for Biomedical
Research, Inc., Cambridge, MA; [4]Barbara Ann Karmanos Cancer Institute, Wayne State University, Detroit, MI, USA

Abstract. A proteomic characterization of one premalignant (MCF10AT1) and two malignant (MCF10CA1a and MCF10 CA1d) human breast cancer cell lines has been performed using a combination of two-dimensional liquid separations and mass spectrometry. Chromatofocusing (CF) and NPS-RP-HPLC are combined with ESI-TOF-MS to resolve and detect intact proteins. Simultaneously, fractions are collected and digested for protein identification using MALDI-MS peptide mass fingerprinting. Following protein identification a small database was compiled for use in comparison between IDs and measured masses taking into account variables such as pI, hydrophobicity and potential modifications. Out of 239 mass bands detected between pH 4.6 and 6.0, 133 have been definitively associated with identified proteins and 67 show consistent up/down regulation in two malignant breast cancer cell lines relative to the precursor premalignant cell line. Of these, 8 are also altered in the premalignant MCF10AT1 cell line by treatment with estradiol. Differentially expressed proteins indicate significant changes to the cytoskeleton, cellular metabolism, and adaptation to environmental stressors in malignant cell lines.

Introduction

With breast cancer widely acknowledged as a major public health issue, scientists have long sought better, more detailed information about the changes at a cellular level that give rise to tumors. The genomic revolution has provided researchers with a number of tools for probing genetic information, from sequencing genes and locating mutations to mRNA expression profiling. While of great value for determining risk or categorizing tumors, these genetic and mRNA data provide only a partial picture of cell biology. The proteins encoded by these genes, in their fully expressed and modified forms, are the molecules responsible for the final malignant nature of cancer cells.

Differential expression can be a result of disease, drug treatment, or differences between the cells such as imprecise tissue sampling or differences between cell lines. In the interest of isolating these differences to disease state or potential therapeutic treatments, the MCF10 xenograft model of human breast cancer was developed (1). Cell lines from this model encompass the entire range of human breast cancer progression from normal tissue to malignant, metastatic tumors. This work will describe differences in acidic protein expression between three of those cell lines, MCF10AT1 (AT1), MCF10CA1a.cl1 (CA1a) and MCF10CA1d.cl1 (CA1d). AT1 cells form simple ductular structures in immune deficient mice that eventually give rise to tumors in about 25% of the xenografts (2). Because progression is possible but not assured, AT1 represents a starting phenotype for progression. CA1a and CA1d are malignant lines derived from tumors originating from AT1 cells. CA1a and CA1d both represent aggressive late-stage phenotypes that lead to rapid tumor growth, morbidity, and metastases (3).

Various top-down proteomics techniques allow researchers to take snapshots of cellular protein expression and study different cellular or disease states. The two-dimensional liquid separation methodology employed here (4) compliments more traditional techniques, such as 2-D-polyacrylamide gel electrophoresis (5,6), by providing similar information (protein molecular weight and pI) together with improved compatibility with mass spectrometry. Cells are lysed and soluble intact proteins fractionated using chromatofocusing, a high-performance column based pH separation technique (7). Protein fractions are then separated by hydrophobicity using nonporous silica reverse phase high pressure liquid chromatography (NPS-RP-HPLC) in conjunction with electrospray ionization time-of-flight mass spectrometry (ESI-TOF-MS) and fraction collection for peptide mass fingerprinting (PMF) by matrix assisted laser desorption ionization time-of-flight mass spectrometry (MALDI-TOF-MS) (8). The end result is an annotated map of protein expression that provides mass, pI and identity. From this map differential protein expression can be quantified for biomarker elucidation.

Previous studies involving these cell lines (9) employed the Bio-Rad Rotofor™ pI separation technique. Although useful

---

Correspondence to: Dr Fred R. Miller, Barbara Ann Karmanos Cancer Institute, 10 E. Warren Ave., Detroit, MI 48236, USA
E-mail: millerf@karmanos.org

for separating preparative quantities of proteins, this approach was susceptible to significant protein overlap and subsequent analyses were often complicated by the complex run buffer employed. In addition, recent advances in automated data analysis (10,11) have allowed a more thorough analysis of several adjacent fractions. As such this work will be the first to compare a broad pI range for MCF10 cells comparing malignant phenotypes (CA1a and CA1d) against an early stage of progression (AT1).

Materials and methods

Cell culture and lysis. CA1a and CA1d cells were grown as monolayers on plastic in Dulbecco's modified Eagle's medium (DMEM)/F12 medium supplemented with 5% horseserum, 10 mM N-2-hydroxyethylpiperazine-N-2-ethanesulfonic acid (HEPES) (pH 7.2). Because the premalignant AT1 cells are not as growth factor independent as are the malignant cells, medium for AT1 growth was further supplemented with 10 μg/ml insulin, 20 ng/ml epidermal growth factor, and 0.5 μg/ml hydrocortisone. Adherent cells were harvested in log phase (~75-80% confluence). The growth medium was aspirated; the cells were gently washed with sterile phosphate buffered saline (pH 7.4), scraped with a rubber policeman, and stored at -80˚C until analysis.

Frozen cell pellets were thawed in 1 ml of lysis buffer containing 7.5 M urea, 2.5 M thiourea, 2% w/v ß-octyl-glucopyranoside, 2 mM phenylmethylsulphonylfluoride, 10% v/v glycerol (all from Sigma-Aldrich, St. Louis, MO, USA) and 10 mM Tris (2-carboxyethyl)phosphine hydrochloride (TCEP) (Pierce Biotechnology, Rockford, IL, USA). Cells were then vortexed for 2 min and lysed over 1 h at room temperature with occasional vortexing. The soluble protein fraction was separated from cell debris via centrifugation at 25,000 x g for 30 min. In order to facilitate buffer exchange and removal of ß-octyl-glucopyranoside, Tris and other potential interference, the supernatant was then diluted to 3 ml with the CF start buffer described below. The sample was then loaded into an Amersham Bioscience PD-10 column (Piscataway, NJ, USA), pre-equilibrated with the start buffer according to the manufacturer's instructions. Start buffer was then added to the column in seven 0.5 ml aliquots, the first aliquot was discarded, and the remaining effluent collected for quantitation. Combined eluent was quantified using a Bradford-type protein assay (Bio-Rad, Hercules, CA, USA) and a Shimadzu UV-1601 Spectrophotometer (Columbia, MD, USA). Bovine serum albumin standards (Sigma) were prepared from 0.17 mg/ml to 1.4 mg/ml in start buffer and analyzed in duplicate at 595 nm alongside the eluent according to the manufacturer's instructions. Eluent was stored at -80˚C unless immediately followed by first dimension (pI) separation.

Chromatofocusing. First dimension (pI) separations were carried out on a Beckman System Gold (Beckman-Coulter Fullerton, CA, USA) using a Beckman-Coulter PS-CF column equilibrated at room temperature with the start buffer containing 6 M urea and 25 mM bis-tris propane adjusted to pH 7.4 using saturated iminodiacetic acid (all Sigma). The separation was monitored by UV absorbance at 280 nm and

pH using an inline flow cell (Lazar Systems, Los Angeles, CA). Using results from the protein assay between 4 and 5 mg of soluble protein were loaded on the column. Once the UV absorbance and pH data stabilized, elution buffer containing 6 M urea and 10% (v/v) Polybuffer 74 (Amersham) was introduced to the column at 0.2 ml/min, creating the pH gradient that drives the separation. Fractions were collected manually every 0.2 pH units until the lower pH limit (~4) was reached. Fractions were then frozen at -80˚C pending analysis and the column was washed sequentially with 1 M NaCl, deionized water, and isopropanol to remove any non-eluted protein.

NPS-RP-HPLC and ESI-TOF-MS. Non-porous-silica reverse phase HPLC (NPS-RP-HPLC) separations were carried out on a 33x4.6 mm Beckman-Coulter NPS-C18 column and Beckman Gold HPLC (Beckman-Coulter) connected to a Micromass/Waters LCT ESI-TOF-MS (Milford, MA). Prior to analysis, the pH of each fraction was verified using a mini-electrode (Fisher) and 1 μg bovine insulin (Sigma, MW=5435) was added to the samples as an internal standard. LCT mass calibration was performed externally using a NaI/CsI standard, yielding a mass accuracy of ~200 ppm for intact proteins. Separations use a water/acetonitrile gradient at 0.5 ml/min with 0.1% trifluoroacetic acid and 0.3% formic acid modifiers (Sigma) as well as the following gradient; prerun 5% B; 0 min, 15% B; 1 min, 25% B; 3 min, 31% B; 6 min, 41% B; 16 min, 47% B; 19 min, 67% B; 23 min, 100% B; 24 min, 100% B; 27 min, 5% B. Blank gradients were run between separations to reduce carryover. Effluent from the column was split with a Quick-Split flow splitter (Analytical Scientific Instruments, El Sobrante, CA) directing 0.3 ml/min to the UV detector for fraction collection and 0.2 ml/min to the LCT for intact mass determination. Individual peaks, absorbance maxima as identified by users at 280 nm, were isolated with a fraction collector (Beckman model SC100) controlled by in-house data acquisition software.

Analyses of ESI-TOF-MS data were carried out with Protein Trawler (BioAnalyte, Inc., South Portland, ME) in conjunction with Masslynx 4.0 (Waters). Trawler automates integration and deconvolution of LC-MS datasets providing retention time, mass and intensity data for intact proteins. Chromatograms were integrated in 45-sec time segments, and the mass range between 800 and 3200 Da was deconvoluted from 4 to 75 kDa with 2 Da resolution. Deconvoluted peak intensities were normalized against the insulin internal standard intensity for each chromatogram. Corrected mass lists were then converted into 2-D mass maps using ProteoVue and DeltaVue (Beckman-Coulter).

MALDI-TOF-MS/PMF. Prior to digestion HPLC fractions were concentrated to ~80 μl using a SpeedVac (LabConCo, Kansas City, MO, USA), then neutralized with 20-60 μl 1 M NH$_4$HCO$_3$ (depending on the original fraction volume). Collected fractions were digested overnight at 37˚C using 0.5 μg sequencing grade modified porcine trypsin (Promega, Madison, WI, USA). Following digestion, peptides were concentrated to ~20 μl using the SpeedVac. Peptides were then desalted using C18 ZipTip™ solid phase extraction micropipette tips (Millipore, Billerica, MA, USA). Peptides
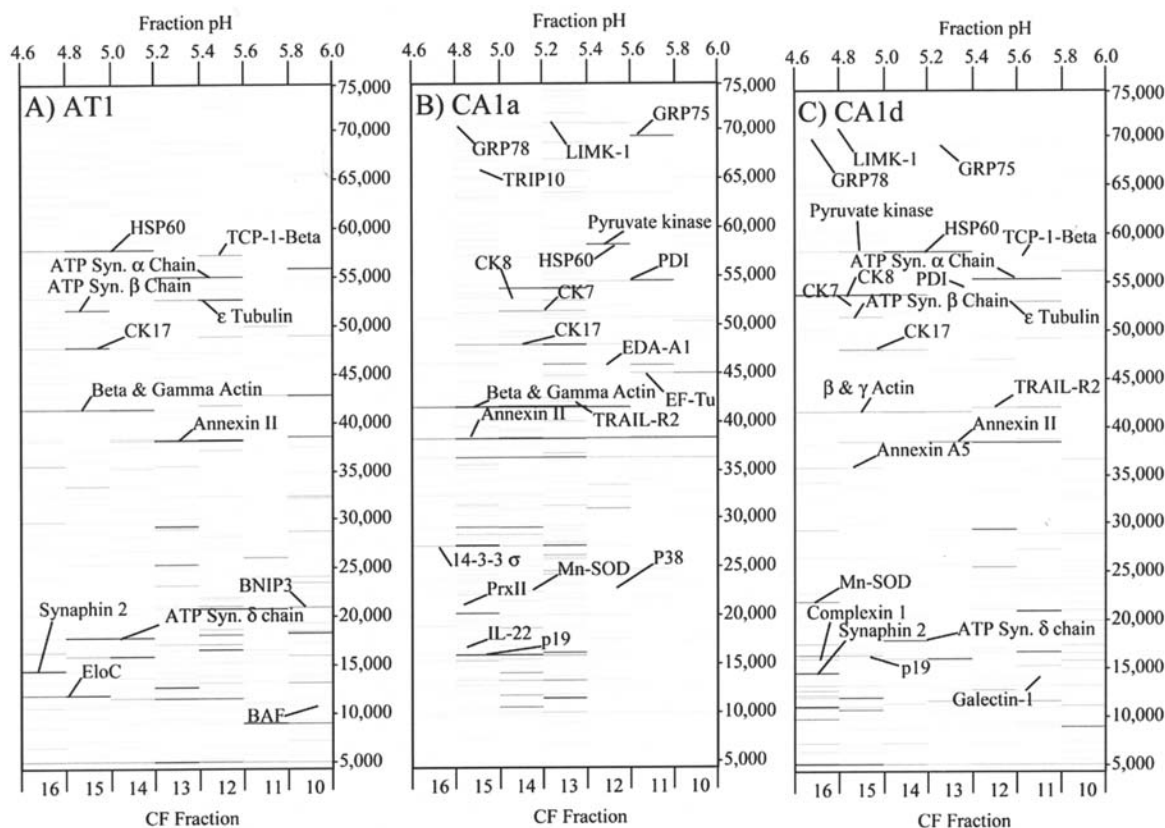
Figure 1. 2-D mass maps of MCF10 cell lines in pH 4.6-6.0 with some protein IDs labeled. A, MCF10AT1; B, MCF10CA1a; C, MCF10CA1d.

were extracted according to manufacturer's instructions and eluted into 7 μl of 60:40 MeCN:H$_2$O with 0.1% trifluroacetic acid.

Desalted peptide (2 μl) was co-crystallized on a MALDI target along with 1 μl of an internal standard/matrix solution containing a 1:3 dilution of saturated α-cyanohydroxycinnamic acid, 0.1 μg of angiotensin (MW=1296 Da), 0.5 μg adrenocorticotropic hormone peptides 1-16 (MW=2093 Da), and 0.5 μg adrenocorticotropic hormone peptides 16-37 (MW=2465), all from Sigma. The target was allowed to air dry before introduction into the source region of a Micromass TofSpec2E MALDI-TOF-MS. Between 20 and 30 spectra were acquired and integrated for each sample. When possible a linear internal calibration was performed using the three peptide standards, if those peptides were suppressed a 'lock mass' spot can be employed to provide a pseudo-internal calibration. True internal calibration routinely yields mass accuracy of 20 ppm or better, with slightly lower mass accuracy for lockmass calibration.

Lists of peptide masses were generated using MassLynx 4.0 and submitted to Protein Prospector (12) for comparison against the SwissProt database (13). Searches were carried out with the following limits: mammals only, pI: 1-10, mass accuracy = 50 ppm, missed cleavages = 2, unmodified cystiene, possible modifications = phosphorylation, acetylation, and methonine oxidation. Results with MOWSE scores >1000 and percent coverage >20% were generally considered good matches for this technique. Given the degree of coelution observed in the second dimension separations unmatched peptides were searched for additional matches. Identities

were then organized by molecular weight and their SwissProt database entries searched for potential isoforms and modifications. Because modifications, isoforms, and alternative splices were extremely common in eukaryotic systems, this step was essential for mass/ID correlation. Relying primarily on published isoforms, as well as post-translational modifications suggested by mass differences, the annotated list of theoretical molecular weights was used to create a final annotated virtual 2-D gel and list of differentially expressed proteins.

Results

Utilizing LC-MS data sets, mass maps (Fig. 1) were created for AT1, CA1a, and CA1d. These maps were then normalized internally using insulin standards, and against one another based on total protein loading for a given CF run. Datasets were then compared against one another manually in 10 kDa increments looking for significant common features using DeltaVue. The resulting list of differentially expressed masses was then compared against a database of annotated MALDI-PMF results with respect to theoretical MW, potential post-translational modifications, pI, and % B. In cases where a protein was not present in one of the cell lines, the lowest overall reportable value (100 counts) was used for purposes of comparison.

Proteins listed in Tables I and II are present in at least two cell lines and are correlated to a confident ID and mass. In several instances, isoforms and post-translational modifications were detected that could not have been identified without the mass resolution of ESI-TOF. Acetylations (+42 Da) appear to

Table I. Proteins up-regulated in malignant MCF10CA1 cell lines.[a]

Exp. MW	Theo. MW	Difference CA1a	CA1d	Accession number	Protein name (+ modifications)
16834	16829	995	105	Q9GZX6	Interleukin-22 precursor (IL-22)
16874	16871	394	30	Q9GZX6	IL-22 + acetyl
68771	68759	373	17	P38646	Stress-70 protein, mitochondrial precursor (GRP75) (Mortalin) + acetyl
29602	29598	286	60	P25786	PROS-30
54308	54298	235	33	P30101	Protein disulfide isomerase A3 precursor (ERp60) + acetyl
45866	45856	216	10	Q9UNE0	Tumor necrosis factor receptor superfamily member EDAR precursor (EDA-A1 receptor)
17103	17101	189	46	O95257	Growth arrest and DNA-damage-inducible protein GADD45 γ + phos
51340	51367	165	104	P08729	Keratin, type II cytoskeletal 7 (cytokeratin 7) (K7) (CK7) (sarcolectin) + phos
45944	45936	130	13	Q9UNE0	EDA-A1 receptor + phos
74810	74798	61	2	P23469	Protein-tyrosine phosphatase ε precursor (R-PTP-ε), isoform 2 + GlcNAc
16429	16426	51	135	O95881	Thioredoxin-like protein p19 precursor (endoplasmic reticulum protein ERp19)
23223	23236	40	30	Q9Y3B8	Oligoribonuclease, mitochondrial precursor (CGI-114), isoform 2
42204	42203	37	31	O14763	Tumor necrosis factor receptor superfamily member 10B precursor (TRAIL-R2), long form
22283	22284	33	144	P04179	Superoxide dismutase (Mn), mitochondrial precursor + phos
12768	12779	32	19	P04436	T-cell receptor α chain V region HPB-MLT precursor + acetyl
55829	55790	31	7	Q13043	Serine/threonine protein kinase 4 (MST-1) + 3 phos
58017	58015	26	83	P14618	Pyruvate kinase, M1 isozyme (CTHBP)
63087	63091	22	3	Q02383	Semenogelin II precursor (SGII) + 2 phos
72683	72681	21	2	P53667	LIM domain kinase 1 (LIMK-1)
23980	23980	21	11	P05814	ß-casine presursor + acetyl
26810	26788	20	3	P51858	Hepatoma-derived growth factor
25477	25492	18	4	Q8WUJ0	Serine/threonine/tyrosine interacting protein (protein tyrosine phosphatase-like protein)
45109	45106	16	10	Q96LI6	Heat shock transcription factor, Y-linked (HSF2-like)
36836	36844	14	6	P42330	Aldo-keto reductase family 1 member C3
73717	73709	14	7	P42680	Tyrosine-protein kinase Tec + 1 phos
68028	68041	13	3	Q9H2D6	TRIO and F-actin binding protein (protein tara)
64604	64591	13	2	P12035	Keratin, type II cytoskeletal 3 (cytokeratin 3) (K3) (CK3) (65 kDa cytokeratin) + phos
66504	66489	13	3	P20700	Lamin B1 + phos
19957	19953	12	6	P01570	Interferon α-14 precursor (interferon α-H) (LeIF H)
64519	64511	12	4	P12035	Keratin, type II cytoskeletal 3 (cytokeratin 3) (K3) (CK3) (65 kDa cytokeratin)
53620	53623	11	8	P05787	Keratin, type II cytoskeletal 8 (cytokeratin 8) (K8) (CK8) + phos
69642	69633	11	2	O60506	Heterogeneous nuclear ribonucleoprotein Q (hnRNP Q)
26456	26428	10	5	P21266	Glutathione S-transferase Mu 3 (GSTM3-3) (GST class-mu 3) (hGSTM3-3)
20725	20733	9	11	P80188	Neutrophil gelatinase-associated lipocalin precursor (NGAL) (P25)
34124	34095	9	3	P06493	Cell division control protein 2 homolog (p34 protein kinase) (CDK1)
47971	47974	9	2	Q04695	Keratin, type I cytoskeletal 17 (cytokeratin 17) (K17) (CK17) (39.1)
71420	71431	9	7	Q16549	Proprotein convertase subtilisin/kexin type 7 precursor + isoform + phos
72711	72681	9	3	P53667	LIMK-1 + phos
54324	54314	8	2	P30101	Protein disulfide isomerase A3 precursor (ERp60) + acetyl + Mox
19320	19340	6	2	P20827	Ephrin-A1 precursor (EPH-related receptor tyrosine kinase ligand 1) (LERK-1)
73781	73789	6	4	P42860	Tyrosine-protein kinase Tec + 2 phos
70527	70521	6	34	P11021	78 kDa glucose-regulated protein precursor (GRP78)
21901	21892	5	2	P32119	Peroxiredoxin 2 (thioredoxin peroxidase 1)
68823	68801	4	4	P38646	GRP75 + 2 acetyl
59699	59671	3	2	P48643	T-complex protein 1, ε subunit (TCP-1-ε) (CCT-ε)
50029	50094	3	10	Q9NY65	Tubulin α-8 chain (α-tubulin 8)
11649	11665	2	8	P05387	60S acidic ribosomal protein P2
12504	12473	2	3	Q15369	Transcription elongation factor B polypeptide 1 (elongin C) (EloC)
20634	20645	2	2	O96000	NADH-ubiquinone oxidoreductase PDSW subunit (complex I-PDSW) (CI-PDSW)
12811	12821	2	5	P04436	HPB-MLT + 2 acetyl
14771	14758	2	5	O15540	Fatty acid-binding protein, brain (B-FABP) (brain lipid-binding protein) (BLBP)

[a]Experimental molecular weights, theoretical molecular weights, fold differences relative to MCF10AT1, accession numbers, and protein name with detected post-translational modifications are indicated.

Table II. Proteins down-regulated in malignant MCF10CA1 cell lines.[a]

Exp. MW	Theo. MW	Fold difference		Accession number	Protein name (+ modifications)
		CA1a	CA1d		
20651	20655	-2	-6	P62256	Ubiquitin-conjugating enzyme E2 H (ubiquitin-protein ligase H)
62683	62681	-2	-10	P31948	Stress-induced-phosphoprotein 1 (STI1) (Hsp70/Hsp90-organizing protein) + acetyl
29478	29543	-2	-39	P06748	Nucleophosmin, isoform 2
32621	32617	-5	-14	P06748	Nucleophosmin (NPM), isoform 1 + acetyl
44454	44460	-6	-4	Q8NBS9	Thioredoxin domain containing protein 5 precursor (thioredoxin-like protein p46)
51849	51849	-6	-10	P06576	ATP synthase ß chain, mitochondrial precursor active form + phos
18451	18444	-6	-3	O75947	ATP Syn D + 2 acetyl
71372	71396	-10	-5	P11021	78 kDa glucose-regulated protein precursor (GRP78), isoform
35962	35967	-17	-3	Q99729	Heterogeneous nuclear ribonucleoprotein A/B (hnRNP A/B)
32851	32851	-20	-8	P07951	Tropomyosin ß chain (tropomyosin 2) (ß-tropomyosin)
24628	24610	-33	-33	P14678	Small nuclear ribonucleoprotein associated proteins B and B' (snRNP-B)
50183	50151	-37	-4	Q9Y6N5	Tubulin α-1 chain (α-tubulin 1)
21541	21541	-41	-36	Q12983	BCL2/adenovirus E1B 19-kDa protein-interacting protein 3 (BNIP3)
26575	26580	-42	-3	P60174	Triosephosphate isomerase (TIM) + acetyl
56024	56009	-154	-154	P00367	Glutamate dehydrogenase 1, mitochondrial precursor (GDH)
55208	55209	-204	-4	P25705	ATP synthase α chain, mitochondrial precursor

[a]Experimental molecular weights, theoretical molecular weights, fold differences relative to MCF10AT1, accession numbers, and protein name with detected post-translational modifications are indicated.
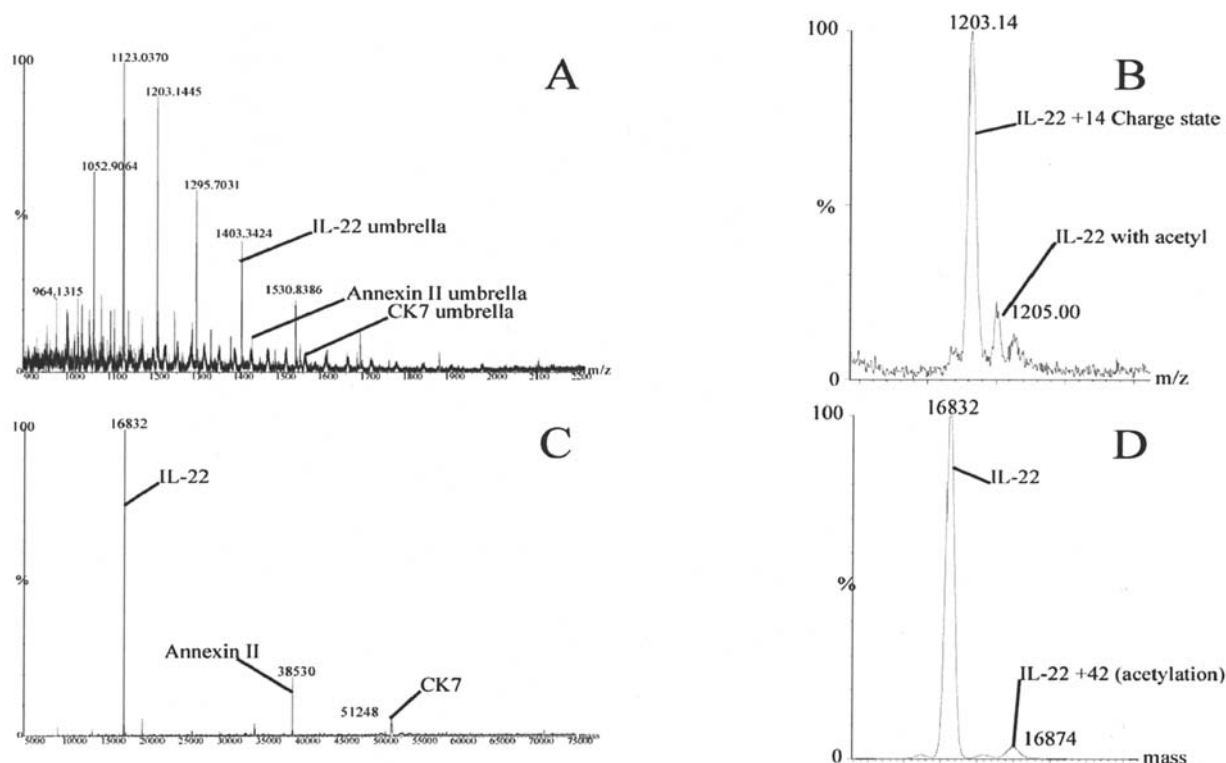

Figure 2. Acetylation of IL-22. A, Raw m/z spectrum of IL-22 and co-eluting proteins. B, Enlargement of labeled IL-22 peak showing acetylation. C, Deconvoluted mass and intensity of IL-22. D, Enlargement of IL-22 intact mass peak showing main peak and +42 Da mass shift of the probable acetylation.

be quite common, more so than suggested by either the protein databases or MALDI-PMF results. One example of such an acetylation is shown in Fig. 2 for IL-22. Although the MALDI-

PMF spectrum for IL-22 (not shown) does not indicate an acetylated peptide, all other important criteria (mass, pI, and retention time) reinforce the ID. Similar examples were located
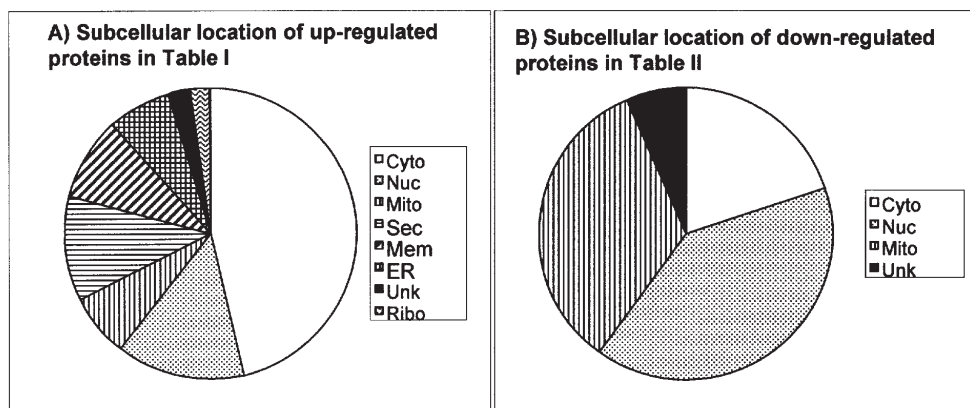
Figure 3. Subcellular locations of up- and down-regulated proteins. Cyto, cytoplasmic; Nuc, nuclear; Mito, mitochondrial; Sec, secretory; Mem, membrane; ER, endoplasmic reticulum; Unk, unknown; Ribo, ribosomal.

for phosphorylated proteins as well. Detected mass shifts of +42 or +80 Da were included in theoretical masses even if the PTM was not explicitly listed in the database. Although hypothetical, these apparent post-translational modifications allowed mass correlations and quantitation that might not otherwise be observed. In the process of making comparisons between cell lines, efforts focused on discovering common features between the cell lines. A total of 239 common mass bands were detected of which 133 were confidently correlated to an identified protein. Of these observed proteins, 67 proteins and isoforms shown in Tables I and II changed with progression to malignancy in both CA1a and CA1d. These proteins are differentially expressed (>2-fold) in both malignant cell lines compared to the premaligant AT1.

An initial attempt to understand the impact of the observed malignancy related changes was carried out by examining the subcellular locations of differentially expressed proteins. Based on SwissProt database entries the subcellular locations for identified proteins are shown in Fig. 3. Cytosolic and nuclear proteins make up the majority of up-regulated proteins, whereas most down-regulated proteins are located in the nucleus and mitochondria. This strongly suggested significant alterations to the cell cycle as well as structure and metabolism.

Differentially expressed proteins were also classified according to their functions as given by SwissProt. Despite the large number of detected proteins, many of these changes represent discrete categories of alterations. The first and most obvious are a broad group of structural changes as seen by changes in expression of cytokeratins, tubulin, and proteins related to actin remodeling, such as LIMK-1 and tropomyosin. Malignant cells also show evidence of stress adaptations by up-regulating protein disulfide isomerase, peroxiredoxin, and several heat shock proteins. Finally, there appear to be significant alterations to metabolism, as seen by the down-regulation of several ATP synthase (ATPase) subunits indicating a downturn in oxidative phosphorylation.

Cytokeratins are a ubiquitous class of cytoskeletal structural proteins found in epithelial cells (among many other types). As reported previously, changes in CK expression have been noted in the MCF10 model (9). CK7 and CK8 were again detected as up-regulated, although it now appears CK17 is up-regulated as well. This is likely related to the analysis of multiple adjacent pI fractions in the present study which

would minimize the impact of band broadening in the pI dimension. CK8 presence has been linked to aggressive phenotypes in both breast and non-small cell lung cancers. In breast cancer it is associated with positive node status, a strong indicator for metastasis and the corresponding poor prognosis (14). Large scale clinical tissue screen has also associated these cytokeratins with abnormal phenotypes, further suggesting their utility as markers (15).

Although (ß and γ) actin expression is only up-regulated in CA1a (data not shown), actin dynamics play a vital role in cell motility and rigidity. LIMK-1, up-regulated 21x and 2x in CA1a and CA1d respectively, participates in actin remodeling by phosphorylating and thereby deactivating cofilin, an actin depolymerizing protein. In MCF7 breast cancer cells, this resulted in a strong correlation to increased invasiveness, a key property for metastasis (16). In addition to the *in vitro* invasiveness assays, Yoshioka *et al* (16) showed a link between LIMK-1 and number and size of osteolytic lesions produced by MDA-MB-231 tumor cells in nude mice. ß-tropomyosin (down-regulated 20x and 8x in CA1a and CA1d respectively) is also of interest in actin dynamics by promoting formation of actin 'stress fibers', which can serve to enhance cell rigidity. Taken together, all these changes strongly suggest the mechanisms by which atypical cells change shape and become more motile.

In order to surmount the various environmental and metabolic stressors tumors encounter, a number of specialized proteins aid in protein synthesis and preservation of cell function. GRP75 and GRP78, both members of the broader 70 kDa heat shock protein (HSP70) family, are molecular chaperones that assist with protein folding and transport, conferring resistance to environmental stressors and playing a role in regulation of cell growth (17). Higher expression of HSP70s has been associated with various cancers, GRP78 in particular has been shown to be associated with resistance to chemotherapeutic agents and is up-regulated in ductal carcinoma *in situ* and invasive ductal carcinoma of the breast (18,19). Additionally, in hepatocarcinomas GRP78 has been associated with increased tumor grade, tumor size, and microvascular invasion (20). Up-regulation of GRP75 increased malignancy of breast cancer cells (21) and antisense to GRP75 induces a senescence-like growth arrest in immortalized human cells (22). Protein disulfide isomerase, also called
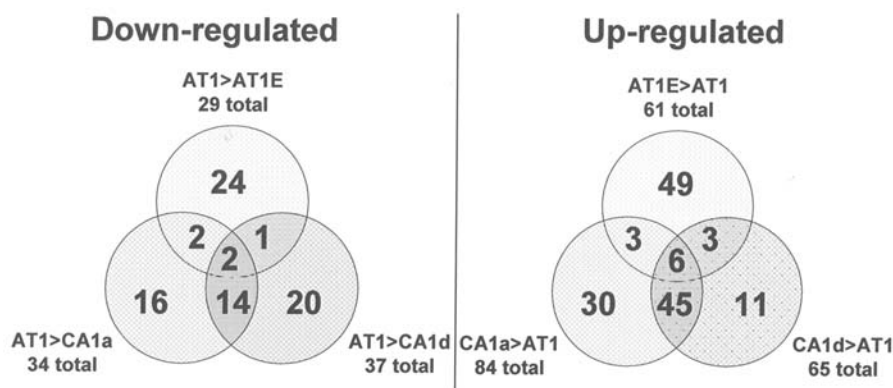
Figure 4. Venn diagrams of common up- and down-regulated proteins in MCF10AT1E, CA1a, and CA1d, relative to MCF10AT1. Circles show the number of proteins differentially expressed relative to AT1, with common proteins included in the intersecting areas.

GRP58 or ERp57, plays a role in protein folding by catalyzing the formation of disulfide bonds. It has been suggested that not only is protein disulfide isomerase up-regulated in various tumors, but it may play a role in the toxicity and specificity of the chemotherapeutic agent Mitomycin C (23).

The second group of proteins involved in stress adaptations is peroxiredoxin 2 (Prx II) and Mn-superoxide dismutase. Each plays a role in scavenging reactive oxygen species, with Mn-superoxide dismutase reducing superoxides to peroxides, and peroxiredoxin further reducing peroxides to water and alcohols. Mn-superoxide dismutase has been well characterized in colorectal carcinoma by Janssen and co-workers, indicating that not only is it up-regulated, but also associated with an negative clinical outcome (24). Peroxiredoxins have also been associated with proliferative and anti-apoptotic phenotypes, although the relationship has limited prognostic value (25).

Metabolic changes, particularly those related to oxidative phosphorylation and glycolysis, are another significant and long-standing area of interest for cancer researchers. Named for its discoverer Otto Warburg, the so-called 'Warburg Effect' is a general observation that tumors show evidence of a significant increase in anaerobic glycolysis (26). In the present work several chains of ATP synthase are seen to be down-regulated together with a corresponding increase in glycolytic enzymes including pyruvate kinase. This significant metabolic shift is believed to represent both an anti-apoptotic mechanism and an adaptation to the hypoxic environment present in most tumors (27). Down-regulation of oxidative metabolism not only reduces the amount of pro-apoptotic superoxide present in cells, but also deprives the cells of excess ATP needed to initiate apoptosis. Taken in conjunction with the increase in pyruvate kinase described here and the up-regulation of fructose bisphosphase aldolase, α enolase, and phosphoglycerate kinase described previously (9), both malignant cell lines have clearly adopted oncogenic glycolysis as a survival strategy (28).

Discussion

A comparison of these data with a previous study of changes induced by estradiol exposure further supports many of these findings (29). MCF10AT1 cells were incubated with estradiol

Table III. Proteins altered in malignant lines and in pre-malignant cells treated with estrogen relative to untreated MCF10AT1.

Up-regulated in AT1e2, CA1a, and CA1d
    Thioredoxin-like protein p19 precursor (p19)
    Tumor necrosis factor receptor superfamily member 10B precursor (TRAIL-R2)
    Keratin, type II cytoskeletal 8 (CK8)
    Stress-70 protein, mitochondrial precursor (GRP75)
    78 kDa glucose-regulated protein precursor (GRP78)
    LIM domain kinase 1 (LIMK-1)

Down-regulated in AT1e2, CA1a, and CA1d
    BCL2/adenovirus E1B 19-kDa protein-interacting protein 3 (BNIP3)
    ATP synthase α chain, mitochondrial precursor

Common in AT1e and CA1a
    Up: Proto-oncogene C-crk (P38), elongation factor Tu (EF-Tu), Cdc42-interacting protein 4 (TRIP10)
    Down: Barrier to autointegration factor (BAF)

Common in AT1e and CA1d
    Up: Galectin-1, Complexin 1, Annexin A5
    Down: 14-3-3 Sigma

---

prior to harvesting and analysis using the 2-D liquid separation methodology described here. This estrogen induced proteome is referred to as MCF10AT1e2. A number of proteins that are differentially expressed between the untreated proteome (MCF10AT1) and the proteome following treatment with estrogen (MCF10AT1e2) have characteristics consistent with the development of a malignant phenotype (29). The degree of identification overlap between malignant related proteins and estrogen-induced proteins is displayed as the Venn diagrams in Fig. 4. As one might anticipate the malignant lines have more features in common, yet 12 up-regulated and 5 down-regulated proteins were shared between estradiol exposed cells and one or both of the malignant cell lines as seen in Table III.

Several proteins described above as playing an important role in metabolism, structure, and stress adaptation in malignant cells also are induced by estrogen in the premalignant cells, further implicating these processes as highly relevant changes because estrogen treatment accelerates progression of premalignant AT1 xenografts in mice (30). Of particular note in this subset of common proteins are: a) BNIP3, an apoptosis-inducing protein that binds BCL2, that was found to be down-regulated 35-fold by estradiol in AT1 cells (29), was decreased to a similar extent with progression (Table II); b) LIM domain kinase-1 that is induced by estrogen in AT1 (29) and up-regulated in both malignant lines may render cells resistant to apoptosis in addition to altering motility (31). Other proteins altered uniformly in malignant cells and estrogen treated premalignant cells are ATPase α chain (down-regulated) and GRP75, GRP78, CK8, and LIMK-1 (up-regulated). Bio-energetic changes have been observed in cells exposed to estrogen and there are numerous reports of estrogen-induced increases of reactive oxygen species in cells (reviewed in refs. 32,33). Induction of reactive oxygen species has been linked to changes in actin turnover together with an overall increase in invasiveness. These data support many of stress, actin remodeling, and metabolic changes described above.

MCF10AT cells express estrogen receptor (ER) (34) and estrogen accelerates progression of the premalignant xenograft lesions (30). Many human breast cancers are ER-negative and estrogen independent, but the early stages of disease in those individuals may have been estrogen responsive. We hypothesize that estrogen independent carcinomas (represented by the MCF10CA lines in the model) may constitutively express proteins that are altered by estrogen in earlier premalignant stages (such as MCF10AT1). The purpose of this study was to identify genes expressed constitutively in malignant MCF10CA variants that are also induced by estrogen in premalignant MCF10AT1 cells.

Although cancer progression is a well-studied process from a histological perspective, modern analytical techniques are finally able to shed light on specific proteins that are at least partly responsible for malignant phenotypes. CF and automated ESI-TOF data analysis allowed a study of an extended region of the acidic pH range in malignant and pre-malignant cells of the MCF10 human breast disease model. Not only was this study able to take advantage of the higher resolution and cleaner samples afforded by CF, but analysis of multiple adjacent fractions allowed more thorough quantitation. This in-turn improved confidence in quantitation, ensuring fraction overlap would not negatively impact results.

Proteins altered in a single CA1a line may be important for the malignant phenotype of that cell line. Galectin 1 (LGALS1), which is induced by estrogen and is up-regulated in MCF10CA1d but not in MCF10CA1a, mediates ras membrane anchorage and cell transformation and enhances ras signal transduction response to EGF (35). LGALS1 is also increased in human breast epithelial cells by overexpression of erbB2 (36). However, proteins altered in both malignant lines should be more fundamental to acquiring a malignant phenotype.

The combination of high performance separations together with mass spectrometry revealed 67 differentially expressed proteins in both MCF10Ca lines (16 down-regulated and 51 up-regulated) compared to the premalignant MCF10AT1 cells.

Of these, expression of 8 proteins was altered in the pre-malignant cells by estrogen (2 down-regulated and 6 up-regulated). Of the eight proteins, one modulates the ras pathway. Mortalin (GRP75) may decrease ras levels and lower activity of downstream MAP kinase Erk2 (37). Many of the identified proteins are implicated in apoptotic signaling. A protein that is 35-fold lower after estrogen treatment and lower in both malignant lines is the hypoxia-regulated pro-apoptotic BCL2 interacting protein BNIP3 (38). Since BNIP3 induction of hypoxic cell death is inhibited by growth factors EGF and IGF (38), decreased BNIP3 expression may be an important factor in loss of growth factor dependence. LIM domain kinase-1 (LIMK-1) protein may inhibit caspase activation (31), GRP78 is overexpressed in malignant but not benign human breast and provides protection from apoptotic signals (18), and thioredoxin has been found to increase growth, increase sensitivity to growth factors and hormones, and inhibit apoptosis (39). Thioredoxin-like protein p19 displays thioredoxin activities and is a secretory protein (40) suggesting a possible autocrine or paracrine activity. TNFR10B, also known as TRAIL-R2 or DRK5, is up-regulated in CA1 lines and induced by estrogen. Although increased death receptor expression might be expected to render cells more susceptible to TRAIL induced apoptosis, TRAIL-R2 overexpression has been found to be associated with aggressive cancer and poor patient survival (41). TRAIL-R2 is also regulated by estrogen in MCF-7 cells but message and protein levels were both reduced in MCF-7 (42) rather than induced as seen with MCF10AT cells. Of the eight proteins identified as being constitutively altered in premalignant MCF10CA1 cells and estrogen responsive in premalignant MCF10AT1 cells, 1 effects ras signaling and 5 have been implicated in survival by inhibiting apoptosis.

Acknowledgements

References

1. Miller FR: Xenograft models of premalignant breast disease. J Mam Gland Biol 5: 379-381, 2000.
2. Miller FR, Soule HD, Tait L, Pauley RJ, Wolman SR, Dawson PJ and Heppner GH: Xenograft model of progressive human proliferative breast disease. J Natl Cancer Inst 85: 1725-1732, 1993.
3. Santner SJ, Dawson PJ, Tait L, Soule HD, Eliason J, Mohamed AN, Wolman SR, Heppner GH and Miller FR: Malignant MCF10CA1 cell lines derived from premalignant human breast epithelial MCF10AT cells. Breast Cancer Res Treat 65: 101-110, 2001.
4. Yan F, Subramanian B, Nakeff A, Barder TJ, Parus SJ and Lubman DM: A comparison of drug-treated and untreated HCT-116 human colon adenocarcinoma cells using a 2-D liquid separation mapping method based upon chromatofocusing pI fractionation. Anal Chem 75: 2299-2308, 2003.
5. Klose J and Kobalz U: Two-dimensional electrophoresis of proteins: an updated protocol and implications for a functional analysis of the genome. Electrophoresis 16: 1034-1059, 1995.

6. Klose J: Protein mapping by combined isoelectric focusing and electrophoresis of mouse tissues. A novel approach to testing for induced point mutations in mammals. Humangenetik 26: 231-243, 1975.

7. Sluyterman LAA and Elgersma O: Chromatofocusing-isoelectric-focusing on ion-exchange columns. 1. General Principles. J Chromatogr 150: 17-30, 1978.

8. Kachman MT, Wang HX, Schwartz DR, Cho KR and Lubman DM: A 2-D liquid separation/mass mapping method for interlysate comparison of ovarian cancers. Anal Chem 74: 1779-1791, 2002.

9. Hamler RL, Zhu K, Buchanan NS, Kreunin P, Kachman MT, Miller FR and Lubman DM: A two-dimensional liquid-phase separation method coupled with mass spectromic studies of breast cancer and biomarker identification. Proteomics 4: 562-577, 2004.

10. Buchanan NS, Hamler RL, Leopold PE, Miller FR and Lubman DM: Mass mapping of cancer cell lysates using two-dimensional liquid separations, electrospray-time of flight-mass spectrometry, and automated data processing. Electrophoresis 26: 248-256, 2005.

11. Williams TL, Leopold P and Musser S: Automated postprocessing of electrospray LC/MS data for profiling protein expression in bacteria. Anal Chem 74: 5807-5813, 2002.

12. Baker PR and Clauser KR. http://prospector.ucsf.edu.

13. Boeckmann B, Bairoch A, Apweiler R, Blatter MC, Estreicher A, Gasteiger E, Martin MJ, Michoud K, O'Donovan C, Phan I, Pilbout S and Schneider M: The SWISS-PROT protein knowledge base and its supplement TrEMBL in 2003. Nucleic Acids Res 31: 365-370, 2003.

14. Brotherick I, Robson CN, Browell DA, Shenfine J, White MD, Cunliffe WJ, Shenton BK, Egan M, Webb LA, Lunt LG, Young JR and Higgs MJ: Cytokeratin expression in breast cancer: phenotypic changes associated with disease progression. Cytometry 32: 301-308, 1998.

15. El-Rehim DMA, Pinder SE, Paish CE, Bell J, Blamey R, Robertson JFR, Nicholson RI and Ellis IO: Expression and co-expression of the members of the epidermal growth factor receptor (EGFR) family in invasive breast carcinoma. J Pathol 203: 661-671, 2003.

16. Yashioka K, Foletta V, Bernard O and Itoh K: A role for LIM kinase in cancer invasion. Proc Natl Acad Sci USA 100: 7247-7252, 2003.

17. Helmbrecht K, Zeise E and Rensing L: Chaperones in cell cycle regulation and mitogenic signal transduction: a review. Cell Prolif 33: 341-365, 2000.

18. Fernandez PM, Tabbara SO, Jacobs LK, Manning FCR, Tsangaris TN, Schwartz AM, Kennedy KA and Patierno SR: Overexpression of the glucose-related stress gene GRP78 in malignant but not benign human breast lesions. Breast Cancer Res Treat 59: 15-26, 2000.

19. Wulfkuhle JD, Sgroi DC, Krutzsch H, McLean K, McGarvey K, Knowlton M, Chen S, Shu HJ, Sahin A, Kurek R, Wallwiener D, Merino MJ, Petricoin EF, Zhao YM and Steeg PS: Proteomics of human breast ductal carcinoma in situ. Cancer Res 62: 6740-6749, 2002.

20. Lim SO, Park SG, Yoo J, Park YM, Kim H, Jang K, Cho JW, Yoo BC, Jung GH and Park CK: Expression of heat shock proteins (HSP27, HSP60, HSP70, HSP90, GRP78, GRP94) in hepatitis B virus-related hepatocellular carcinomas and dysplastic nodules. World J Gastroenterol 11: 2072-2079, 2005.

21. Wadhwa R, Takano S, Kaur K, Deocaris CC, Pereira-Smith OM, Reddell RR and Kaul SC: Upregulation of mortalin/mthsp70/GRP75 contributes to human carcinogenesis. Int J Cancer 118: 2973-2980, 2006.

22. Wadhwa R, Takano S, Taira K and Kaul SC: Reduction in mortalin level by its antisense expression causes senescence-like growth arrest in human immortalized cells. J Gene Med 6: 439-444, 2004.

23. Celli CM and Jaismal AK: Role of GRP58 in mitomycin C-induced DNA cross-linking. Cancer Res 63: 6016-6025, 2003.

24. Janssen AML, Bosman CB, Kruidenier L, Griffioen G, Lamers CBHW, van Krieken JHJM, van de Velde CJH and Verspaget HW: Superoxide dismutases in the human colorectal cancer sequence. J Cancer Res Clin Oncol 125: 327-335, 1999.

25. Noh DY, Ahn SJ, Lee RA, Kim SW, Park IA and Chae HZ: Overexpression of peroxiredoxin in human breast cancer. Anti-cancer Res 21: 2085-2090, 2001.

26. Warburg O: Metabolism of Tumors. Arnold Constable, London, 1930.

27. Cuezva JM, Krajewska M, De Heredia ML, Krajewski S, Santamaria G, Kim H, Zapata JM, Marusawa H, Chamorro M and Redd JC: The bioenergetic signature of cancer: a marker of tumor progression. Cancer Res 62: 6674-6681, 2002.

28. Dang CV and Semenza GL: Oncogenic alterations of metabolism. Trends Biochem Sci 24: 68-72, 1999.

29. Zhao J, Zhu K, Miller FR and Lubman DM: Proteomic analysis of estrogen response of premalignant human breast cells using a 2-D liquid separation/mass mapping technique. Proteomics 6: 3847-3861, 2006.

30. Shekhar MPV, Nangia-Makker P, Wolman SR, Tait L, Heppner GH and Visscher DW: Direct action of estrogen on sequence of progression of human preneoplastic breast disease. Am J Pathol 152: 1129-1132, 1998.

31. Yang E, Kim H, Lee J, Shin JS, Yoon H, Kim SJ and Choi IH: Overexpression of LIM kinase 1 renders resistance to apoptosis in PC12 cells by inhibition of caspase activation. Cell Mol Neurobiol 24: 181-192, 2004.

32. Felty Q, Xiong WC, Sun DM, Sarkar S, Singh KP, Parkash J and Roy D: Estrogen-induced mitochondrial reactive oxygen species as signal transducing messages. Biochemistry 44: 6900-6909, 2005.

33. Felty Q and Roy D: Mitochondrial signals to nucleus regulate estrogen-induced cell growth. Med Hypotheses 64: 133-141, 2005.

34. Shekhar PVM, Chen ML, Werdell J, Heppner GH, Miller FR and Christman JK: Transcriptional activation of functional endogenous estrogen receptor gene expression in MCF10AT cells: a model for early breast cancer. Int J Oncol 13: 907-915, 1998.

35. Paz A, Haklai R, Elad-Sfadia G, Ballan E and Kloog Y: Galectin-1 binds oncogenic Hras to mediate ras membrane anchorage and cell transformation. Oncogene 20: 7486-7493, 2001.

36. Elad-Sfadia G, Haklai R, Ballan E, Gabins HJ and Kloog Y: Galectin-1 augments ras activation and diverts ras signals to Raf-1 at the expense of phosphoinositide 3-kinase. J Biol Chem 277: 37169-37175, 2002.

37. Wadhwa R, Yaguci T, Hasan MK, Taira K and Kaul SC: Mortalin-MPD (mevalonate pyrophosphate decarboxylase) interactions and their role in control of cellular proliferation. Biochem Biophys Res Commun 302: 735-742, 2003.

38. Kothari S, Cizeau J, McMillan-Ward E, Israels SJ, Bailes M, Ens K, Kirshenbaum LA and Gibson SB: BNIP3 plays a role in hypoxic cell death in human epithelial cells that is inhibited by growth factors EGF and IGF. Oncogene 22: 4734-4744, 2003.

39. Powis G, Mustacich D and Coon A: The role of redox protein thioredoxin in cell growth and cancer. Free Radic Biol Med 29: 312-322, 2000.

40. Liu F, Rong Y-P, Zeng L-C, Zhang X and Han Z-G: Isolation and characterization of a novel human thioredoxin-like gene hTLP19 encoding a secretory protein. Gene 315: 71-78, 2003.

41. McCarthy MM, Sznol M, DiVito KA, Camp RL, Rimm DL and Kluger HM: Evaluating expression and prognostic value of TRAIL-R1 and TRAIL-R2 in breast cancer. Clin Cancer Res 11: 5188-5194, 2005.

42. Wang TTY and Jeng J: Coordinated regulation of two TRAIL-R2/KILLER/DR5 mRNA isoforms by DNA damaging agents, serum and 17ß-estradiol in human breast cancer cells. Breast Cancer Res Treat 61: 87-96, 2000.